JOURNAL OF SOLID STATE CHEMISTRY **133,** 31–35 (1997)
ARTICLE NO. SC977312

Structure and Chemistry of the YB_{66}(100) Surface

Craig L. Perkins and Michael Trenary[1]

Department of Chemistry, University of Illinois at Chicago, 845 W Taylor Street, Chicago, Illinois 60607-7061

and

Takaho Tanaka

National Institute for Research in Inorganic Materials, 1-1 Namiki, Tsukuba, Ibaraki, 305, Japan

Received January 21, 1997; accepted February 6, 1997

The structure of the clean YB_{66}(100) surface was studied with X-ray photoelectron spectroscopy, low-energy electron diffraction (LEED), and scanning tunneling microscopy (STM). A clean, well-ordered surface can be prepared by Ar ion bombardment followed by annealing to 1200°C. The fact that heating does not lead to the preferential loss of boron or yttrium indicates that the material evaporates congruently in vacuum. Although the bulk structure of YB_{66} is quite complex with over 1600 atoms per unit cell, both LEED and STM reveal that the surface structure has long-range two-dimensional periodicity described by a simple square lattice. The surface lattice constant determined by LEED is 21±3 Å, whereas the bulk value is 23.44 Å. Large scale images obtained with STM reveal that the surface consists of flat (100) terraces separated by steps 11.7 Å (half unit cell) in height. Smaller scale STM images reveal a 11.7 Å square grid of objects. These objects are identified as icosahedral clusters of 156 boron atoms. In its reactivity toward oxygen, the surface shows behavior similar to that reported for a β-rhombohedral boron (111) surface.

INTRODUCTION

Due to their unusual stoichiometry, complex structure, and interesting physical properties, YB_{66} and other MB_{66} materials have been the subject of several investigations since the discovery of YB_{66} by Seybolt in 1959 (1–5). The structure of these materials is usually described in terms of a "super-icosahedron" consisting of 12 B_{12} icosahedra arranged around a thirteenth central B_{12} unit, resulting in a cluster best written as $B_{12}(B_{12})_{12}$. Eight of these B_{156} super-icosahedra and eight nonicosahedral cages of 48 or 36 boron atoms are arranged in an fcc lattice 23.44 Å on a side and belonging to space group *Fm*3*c*. Adjacent super-icosahedra differ only by a 90° relative rotation around one of the principal axes. Metal atoms and nonicosahedral boron clusters are located in fourfold channels within the B_{156} framework. Although the boron network exhibits little disorder in high-quality crystals, even in the best crystals the metal atoms randomly occupy only about 50% of the available sites (4). While the structure is conveniently described in terms of B_{156} units, it has not been at all clear if these boron super-icosahedra have structural stability as discrete entities within the overall crystal structure, or are merely convenient conceptual constructs used for describing the structure. The latter viewpoint is suggested by the fact that many of the B–B bonds between super-icosahedra are shorter than the bonds within the super-icosahedra. This would imply that the boron atoms are merely part of an undifferentiated extended three-dimensional network.

Although the bulk YB_{66} crystal structure has been repeatedly examined, there have been no published studies on its surface structure. Yet the surface properties of YB_{66} are highly relevant to its use as a superior soft X-ray monochromator (6). The elaborate YB_{66} lattice presents a myriad of possibilities for surface termination, reconstruction, surface electronic structure, and site specific chemical reactivity. Disorder associated with the structure, such as the distribution of the yttrium atoms and some reportedly statistically occupied boron sites (2), is inaccessible to diffraction techniques but may be observable with a real space imaging technique such as scanning tunneling microscopy (STM). For these reasons, we have undertaken a surface science study of YB_{66}(100).

EXPERIMENTAL

Two different single crystal samples were used in these studies. They were grown, cut, and polished at the National Institute for Research in Inorganic Materials in Tsukuba, Japan. The crystals had the congruently melting

[1] To whom correspondence should be addressed.

0022-4596/97 $25.00

composition of YB_{62}. Details of the crystal growth method can be found elsewhere (7). The experiments described here were conducted in a standard UHV surface analysis chamber, details of which have been previously published (8). In short, the apparatus consists of a vacuum chamber (base pressure $< 5 \times 10^{-11}$ Torr) equipped with low-energy electron diffraction (LEED) optics, a quadrupole mass spectrometer (QMS), an STM, a system for X-ray photoelectron spectroscopy (XPS), a sputter ion gun for sample cleaning, and facilities for sample heating and cooling.

Imaging with the STM was performed in a constant current mode at room temperature and was typically initiated 2 h after sample cleaning to minimize thermal drift. Tips for the STM were prepared by electrochemically etching tungsten wire and were cleaned *in situ* by electron bombardment and field desorption. The STM piezo-tube expansion coefficients were determined by obtaining atomically resolved images of a Si(111) (7×7) crystal encompassing regions having one or more steps.

A mild etch (9) was performed on the single crystal YB_{66} samples, which were subsequently mounted in graphite ferrules and placed under vacuum. The principal contaminants, found from XPS to be carbon and oxygen, could be removed with gentle argon ion sputtering (500 eV) and heating to $\sim 1200^{\circ}$C. Temperatures were monitored with an optical pyrometer and were not emissivity corrected. Due to the low thermal conductivity and brittle nature of YB_{66}, samples were heated and cooled slowly (< 0.5 K/s).

The XPS binding energy scale was assumed to be linear and was related to the Au $4f_{7/2}$ and Ag $3d_{5/2}$ binding energies as recommended by Powell (10). Typical survey scans taken from 0–1100 eV demonstrated that the samples could be prepared free of oxygen and carbon ($< 1\%$ of a monolayer), and would remain so for over 8 h (11). Oxygen exposure experiments were performed as follows: the crystal was first cleaned of oxygen and carbon as established by XPS, and then it was dosed with a given amount of oxygen, followed by the acquisition of a spectrum. Oxygen exposures were additive; i.e., the crystal was not cleaned after each exposure.

RESULTS

Since no prior surface science studies of YB_{66} have been reported, it was necessary to first establish what conditions are needed to obtain a clean, well-ordered surface. It was also necessary to establish if repeated heating and/or Ar ion bombardment would alter the surface stoichiometry due to preferential removal of yttrium or boron. It was found by XPS that mild argon ion (500 eV) sputtering reduced the B/Y ratio from its initial value of $\sim 72:1$ to $\sim 35:1$ (12). However, post-sputter annealing to temperatures $> 1200^{\circ}$C restored the stoichiometry to the initial value. The initial sputtering also resulted in some pitting (visible to the eye) of the originally smooth surface. Electron micrographs of the pitted regions revealed a dendritic pit structure. The difference between the surface B : Y ratio as measured by XPS (72 : 1) and that of the bulk (62 : 1) can be at least partially attributed to the use of literature values of the elemental sensitivity factors (13) instead of values specifically calibrated for our XPS system. Annealing the samples to higher temperatures (1400°C) still gave a B/Y ratio of $\sim 72:1$, thus implying that the $YB_{66}(100)$ surface evaporates congruently and may be cleaned repeatedly under UHV conditions without permanent alteration of the material's composition.

After a few cleaning cycles the samples yielded sharp LEED patterns, a typical example of which is shown in Fig. 1 for a beam energy of 38.3 eV. The observed LEED patterns immediately reveal several important features of the $YB_{66}(100)$ surface structure. First, the fact that the spots are extremely sharp with a low background shows that there is a high degree of translational order on a length-scale of 10–100 nm. This is in contrast to the visible pitting of the surface, as noted above, indicating roughness on a length-scale of 10–100 μm. The LEED pattern shown in Fig. 1 is typical of what was observed at various points across the faces of the two separate 12 mm diameter samples studied. Second, the square grid of LEED spots and their spacing for a given beam energy implies that the surface lattice constant is 21 ± 3 Å. This value was based on calibration of the LEED optics with a Si(111) sample. Thus the surface lattice constant is identical to that of a bulk (100) plane. However, due to the large size of the surface unit cell, a variety of surface terminations and reconstructions within the unit cell are consistent with the LEED pattern. Two other features are apparent in the photograph of Fig. 1. Glide plane symmetries present in the YB_{66} lattice manifest themselves as extinctions over the entire range of incident electron

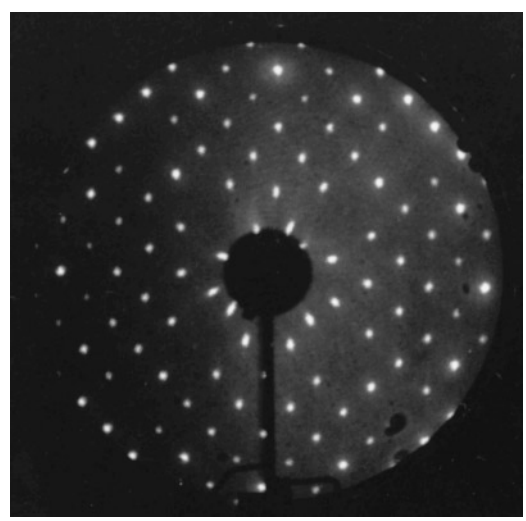

FIG. 1. A typical LEED pattern from $YB_{66}(100)$, taken at 38.3 eV.

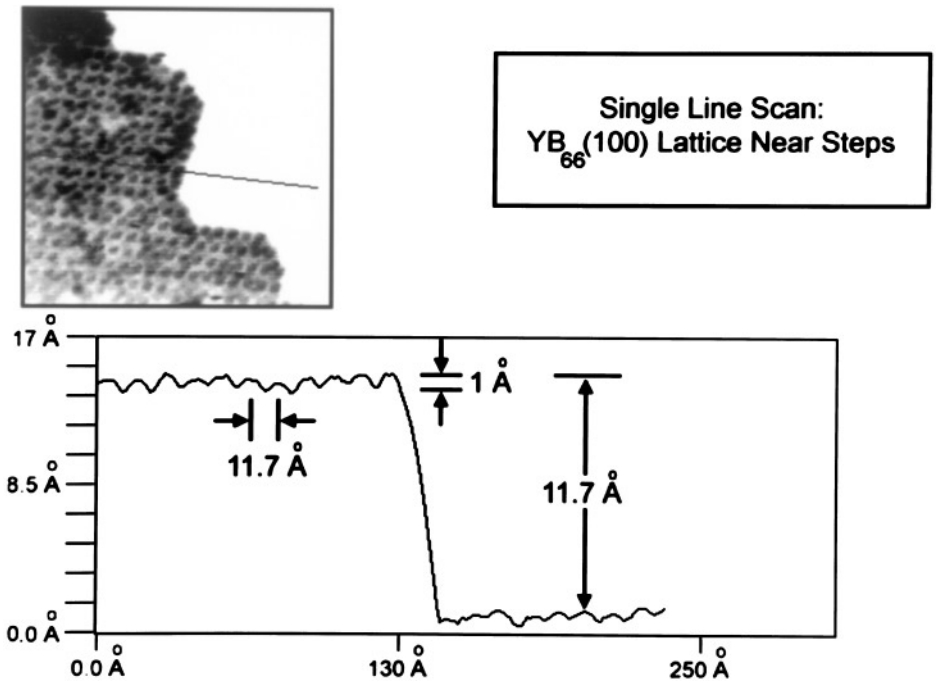

FIG. 2. An STM image of the $YB_{66}(100)$ surface obtained with a bias of -5 V and a setpoint of 0.5 nA taken near a step edge along with a line scan across the steps showing a step height of 11.7 Å and a 1 Å corrugation on the terraces.

energies for $(h, 0)$ and $(0, k)$ spots, where h and k are odd (14). Also, spots toward the center of the pattern show some distortion as a result of fringing fields or stray magnetic fields.

STM topographs of the clean surface revealed large (100) terraces separated by steps of half unit cell height (11.7 Å) (15). Images of individual terraces reveal a square lattice with half unit cell periodicity (15). Figure 2 shows an STM image at a step edge and a line scan across the step. On the upper terrace an 11.7 Å square lattice of objects is observed that extends right up to the step edge. The irregularities at the step edges are seen to consist of whole units of these objects. The corrugation between the entities forming the lattice is seen to be on the order of 1 Å and was found to be independent of the tunneling voltage and bias.

Figure 3 consists of two XPS spectra taken at room temperature with a resolution of about 1 eV: the lower spectrum is of the clean crystal and the upper one was taken after the sample at 700°C had been exposed to 2.6×10^4 L (Langmuir, 1 L $= 1 \times 10^{-6}$ Torr sec) of O_2. All XPS peaks were fit using linear baselines and exponentially tailed Gaussians. The spacing between the $Y(3d_{5/2})$ and $Y(3d_{3/2})$ peaks is large enough that curve fitting can be applied to them individually. Extraction of the $Y(3d_{5/2})$ position allowed estimation of the yttrium oxidation state. Comparing our value of 157.1 ± 0.2 eV to that of the free metal (156.0 eV) (16) and that of the oxide ($\sim$157 eV) (13) indicates that the metal is present in a $+3$ oxidation state. This is in accord with the role generally attributed to metal atoms in the boron-rich solids as donors of electrons to the highly electron-deficient boron network. The B(1*s*) peak of the clean surface is at 187.8 ± 0.2 eV. This value is the lowest measured for any metal boride and, not suprisingly, is essentially the same as the 187.7 eV binding energy measured previously in our laboratory for β-rhombohedral

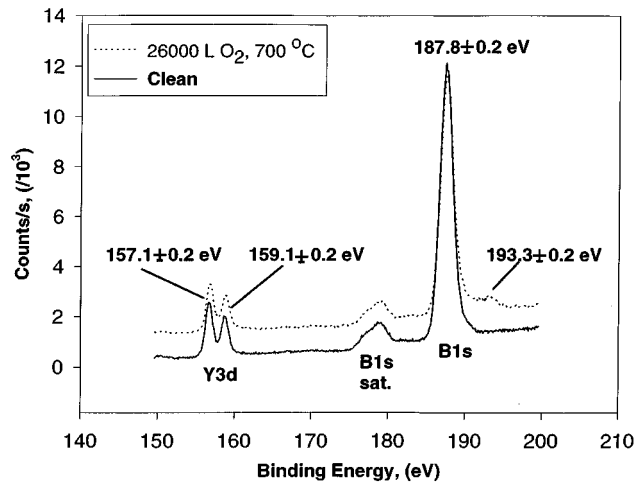

FIG. 3. XPS spectra of the Y(3*d*) and B(1*s*) region for a clean surface and a surface oxidized by exposure to 26,000 L O_2 at a crystal temperature of 700°C.

boron (111) (17). Lastly, the small peak around 179 eV is assigned to an Mg$K\alpha_{3-4}$ radiation satellite of the large B(1*s*) peak.

The spectrum of the surface exposed to oxygen at 700°C in Fig. 3 shows a small hump at 193.3 eV, a value close to the B(1*s*) binding energy of 193.4 eV reported for B_2O_3 (17–18). No chemically shifted boron or yttrium peaks were detectable in the spectra following oxygen exposure at room temperature. The very small ($\sim$0.2 eV) shift of the entire spectrum of the oxidized crystal to higher binding energy is presumably due to charging (17), as this shift was also observed to occur in the O(1*s*) region. The binding energy of the O(1*s*) peak (not shown) was 532.2 ± 0.2 eV, which is close to the value obtained for an oxidized boron surface (17). Samples that had been held at 700°C and exposed to 26,000 L of oxygen still exhibited a dim (1×1) LEED pattern.

Figure 4 shows plots of the O(1*s*) peak area as a function of oxygen exposure for surfaces at room temperature and at 700°C. At both temperatures studied, there seem to be two distinct regimes of oxygen uptake by the YB_{66}(100) surface: below about 3000 L, oxygen is adsorbed relatively quickly, whereas at exposures higher than 3000 L, oxygen is adsorbed more slowly. Considerably more oxygen reacted with the surface at 700°C than at room temperature. At neither temperature did the amount of oxygen at the surface reach a constant saturation value. The temperature and exposure dependence of the oxygen uptake is quite similar to what was observed for the (111) surface of β-rhombohedral boron as is the observation of a small chemically shifted B(1*s*) peak indicative of boron in the same oxidation state as in B_2O_3 (17). The similarities are not surprising since the structures of both YB_{66} and β-rhombohedral boron involve similar icosahedral bonding environments for the boron atoms.

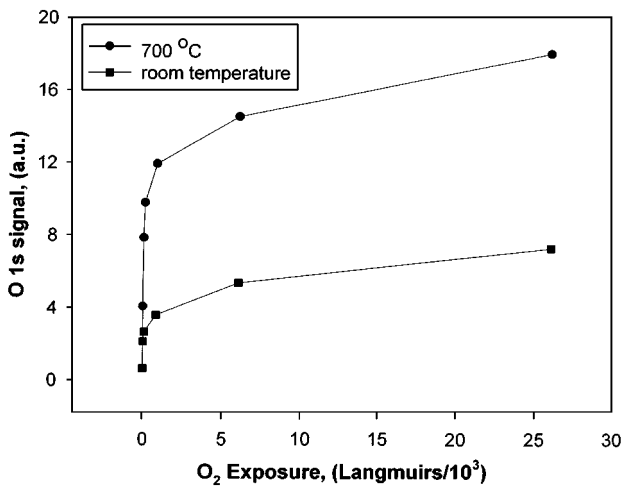

FIG. 4. A plot of XPS O(1*s*) peak areas versus oxygen exposure with the YB_{66} sample at room temperature and at 700°C.

DISCUSSION

The XPS and LEED data presented here demonstrate that a clean well-ordered YB_{66}(100) surface can be readily and reproducibly obtained under UHV conditions. This in turn makes the surface amenable to more detailed study with standard surface science techniques. This basic fact about YB_{66} had not been previously established nor could it have been predicted. For example, the surfaces of many solid compounds undergo a change in composition every time the sample is heated in vacuum. Other surfaces undergo reconstruction to structures with two-dimensional periodicities quite different from the corresponding bulk planes. The absence of such complications for YB_{66}(100) also suggests that studies of its surface structure might clarify aspects of its intrinsically complex bulk structure.

The LEED and STM data can be considered with reference to the idealized bulk terminated (100) YB_{66} plane. The (100) plane has two basic structural units with the full periodicity (23.4 Å) of the bulk, the lattice of B_{156} units, and the lattice of nonicosahedral cages (B_{48} and B_{36} units). The LEED patterns demonstrate that the bulk periodicity is preserved at the surface, while the STM images provide evidence for a surface lattice having half unit cell periodicity (11.7 Å). Although one must be careful in assigning geometric structures to specific features observed in STM images, images of our crystals show no dependence on either the polarity or absolute magnitude of the tunneling bias and most likely are not artifacts produced by sampling specific surface states. The two seemingly contradictory sets of data from the LEED and STM experiments may be reconciled if one makes the assumption that adjacent lattice units appear identical in STM images. This can be justified in the case of the B_{156} lattice, since the lattice is comprised of super-icosahedra of high sphericity, and since adjacent super-icosahedra differ only by a 90° relative rotation. In the case of the lattice of nonicosahedral cages, in which the yttrium atoms are known to be randomly distributed and which is reported to have an intrinsic amount of disorder, it is unlikely that adjacent nonicosahedral units would appear identical in the STM images. Therefore the STM and LEED data point toward the (100) surface as being a square lattice of B_{156} super-icosahedra. The structure observed at the step edges can then be associated with the presence or absence of whole B_{156} units. Furthermore, the step height of 11.7 Å then implies that adjacent terraces are composed of adjacent layers of whole B_{156} units. All of these facts taken together imply that the B_{156} super-icosahedra exist as stable, discrete entities within the solid and thus constitute the basic structural element of YB_{66}. While formal descriptions of YB_{66} are based on such units, this is the first indication that these icosahedral arrangements of 156 boron atoms have an independent physical reality and are anything more than simply a convenient way to represent the structure.

ACKNOWLEDGMENTS

This work was supported by the National Science Foundation, DMR-941037. We thank Dr. Takashi Aizawa of NIRIM for helpful discussions of his unpublished work on the YB_{66}(100) surface.

Note added in proof. Since this paper was first submitted the following additional STM results have been obtained: (1) structure has been observed showing that the two halves of the surface unit cell do not appear identical in some images and that the periodicity implied by STM is the same as implied by LEED and as expected based on the structure of the bulk (100) plane; (2) under certain conditions the images do show a bias voltage dependence; (3) detailed analysis suggests that the lattice objects seen in the STM images do not consist of whole B_{156} units. This additional work will be published elsewhere (11).

REFERENCES

1. A. U. Seybolt, *Trans. Am. Soc. Met*. **52,** 971 (1960).
2. S. M. Richards, Ph.D. thesis, Rensselaer Polytechnic Institute, 1966.
3. S. M. Richards and J. S. Kasper, *Acta Crystallogr. B* **25,** 237 (1969).
4. G. A. Slack *et al*., *J. Phys. Chem. Solids* **38,** 45 (1977).
5. J. S. Kasper, *J. Less Common Metals* **47,** 17 (1976).
6. M. Rowen *et al*., *Synchrotron Radiation News* **6,** (3), 25 (1993).
7. Y. Kamimura, T. Tanaka, S. Otani, Y. Ishizawa, Z. U. Rek, and J. Wong, *J. Crystal Growth* **128,** 429 (1993). [The particular crystals used in these studies also contained a small amount of scandium which was added in an effort to improve the crystal quality]
8. J. Ozcomert, Ph.D. thesis, University of Illinois at Chicago, 1992.
9. The etch solution consisted of the following: 30 g $K_3Fe(CN)_6$, 10 g NaOH, and 150 g of water.
10. C. J. Powell, *Surface Interface Anal*. **23,** 121 (1995).
11. C. L. Perkins, M. Trenary, and T. Tanaka, to be published.
12. The absolute atomic ratios were determined using published XPS elemental sensitivity factors that probably are not correct for our spectrometer. Emphasis should be placed on the relative changes of the atomic ratios observed during cleaning.
13. J. Chastain (Ed.), "Handbook of X-Ray Photoelectron Spectroscopy," Perkin-Elmer Corporation, Physical Electronics Division, Eden Prairie, MN, 1992.
14. M. A. Van Hove, W. H. Weinberg, and C. M. Chan, "Low-Energy Electron Diffraction: Experiment, Theory, and Surface Structure Determination," p. 76. Springer-Verlag, Berlin, 1986.
15. C. L. Perkins, M. Trenary, and T. Tanaka, *Phys. Rev. Lett*. **77,** 4772 (1996).
16. C. J. Powell, *Appl. Surface Sci*. **89,** 141 (1995).
17. W. C. Foo, J. S. Ozcomert, and M. Trenary, *Surface Sci*. **255,** 245 (1991).
18. D. J. Joyner and D. M. Hercules, *J. Chem. Phys*. **72,** 1095 (1980).